Electronic Supplementary Material (ESI) for Nanoscale.

SUPPORTING MATERIALS

Nanoscale dynamical investigation of the hemoglobin complex with the bacterial protein IsdB: is their interaction stabilized by catch bonds?

Valentina Botti[#a], Omar De Bei[#b], Marialaura Marchetti[b], Barbara Campanini[c], Salvatore Cannistraro[a], Stefano Bettati*[b,d] and Anna Rita Bizzarri*[a]

[a] *Biophysics and Nanoscience Centre, DEB, Università della Tuscia, Largo dell'Università, 01100, Viterbo, Italy;* [b] *Department of Medicine and Surgery, University of Parma, Via Volturno 39, 43125, Parma, Italy;* [c] *Department of Food and Drug, University of Parma, Parco Area delle Scienze 23/A, 43124, Parma, Italy;* [d] *Institute of Biophysics, National Research Council, Via Moruzzi 1, 56124, Pisa, Italy*

[#]*Contributed equally*

* *Corresponding authors*

AFS Histograms

Figure S1 and S2 show the histograms of the unbinding forces for the IsdB:metHb complex, at the various loading rates, by using two different binnings.

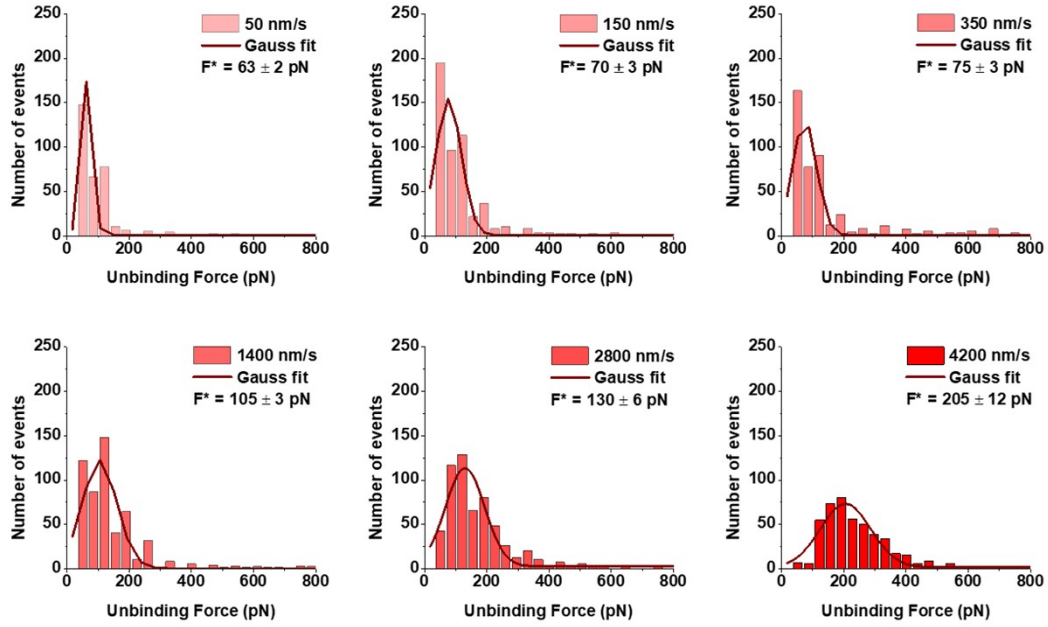

Figure S1. Histograms of the unbinding forces for the IsdB:metHb complex from AFS measurements carried out at increasing retraction velocities, using a binning of 35 nN. Each histogram has been fitted with a Gaussian function (red curve) to determine the most probable unbinding force value (F*) from the peak maximum.

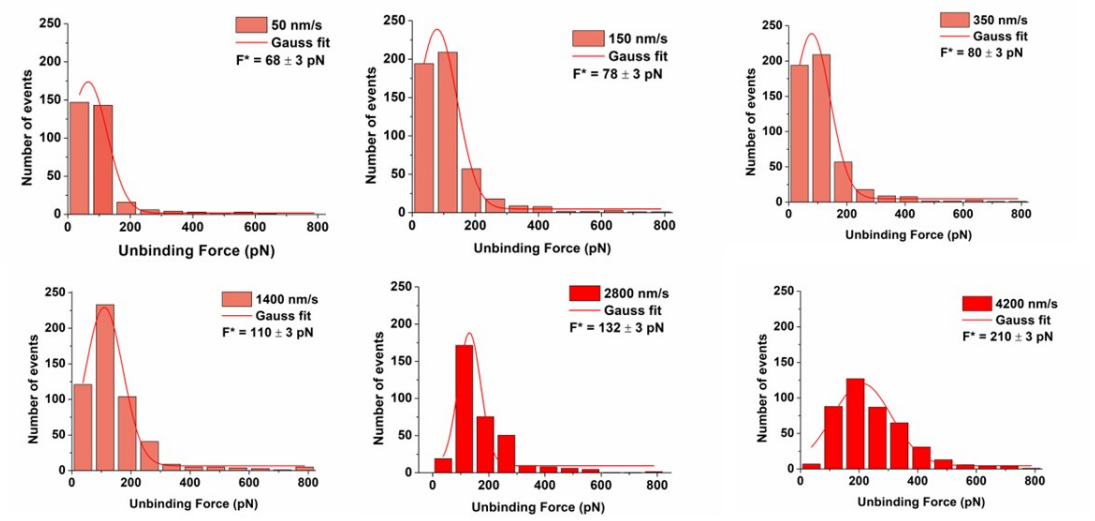

Figure S2. Histograms of the unbinding forces for the IsdB:metHb complex from AFS measurements carried out at increasing retraction velocities, using a binning of 75 nN. Each histogram has been fitted with a Gaussian function (red curve) to determine the most probable unbinding force value (F*) from the peak maximum.

Figure S3 and S4 show the histograms of the unbinding forces for the IsdB:(ββ)XL-Hb complex, at the various loading rates, using two different binnings.

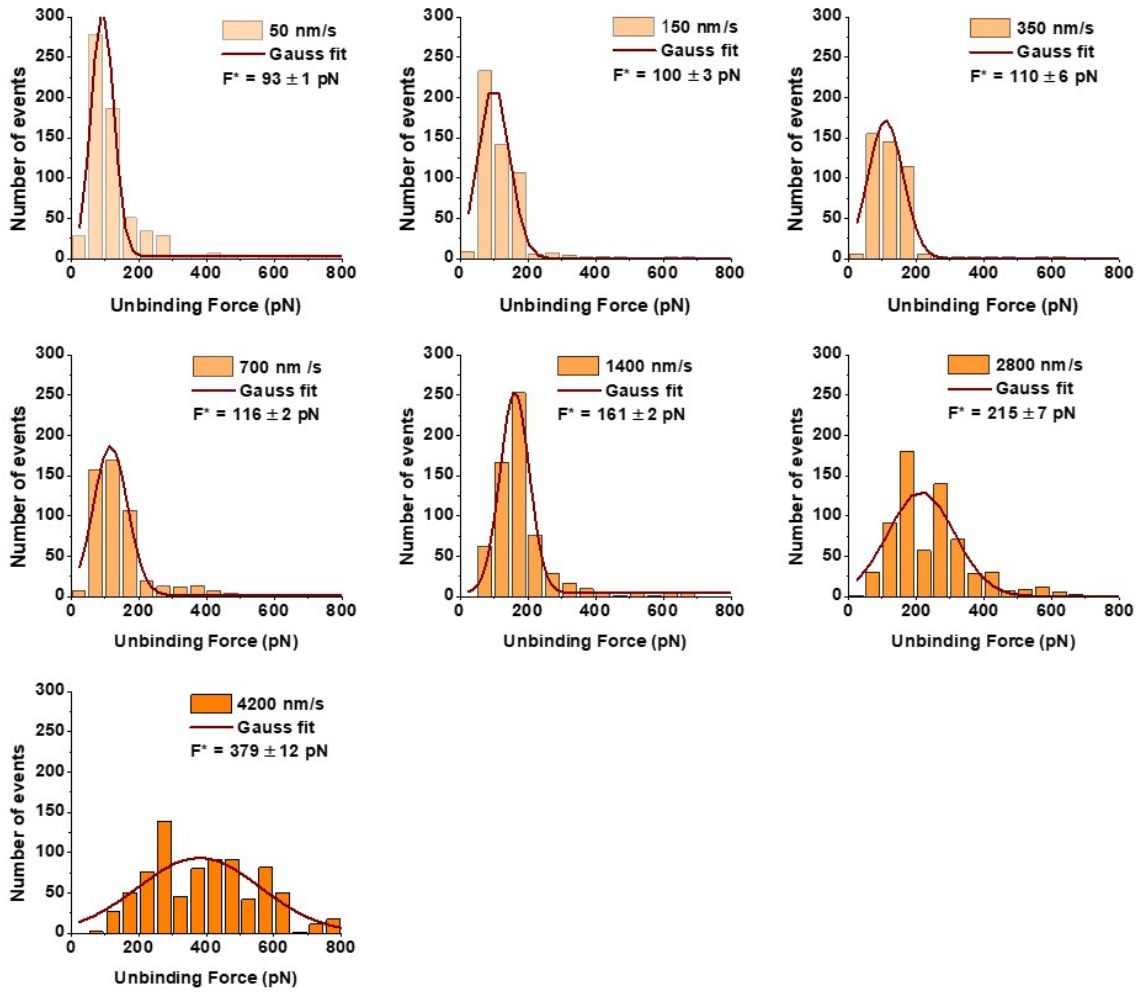

Figure S3. Histograms of the unbinding forces for the IsdB:(ββ)XL-Hb complex from AFS measurements carried out at increasing retraction velocities, using a binning of 35 nN. Each histogram was fitted with a Gaussian function (red curve) to determine the most probable unbinding force value (F*) from the peak maximum.

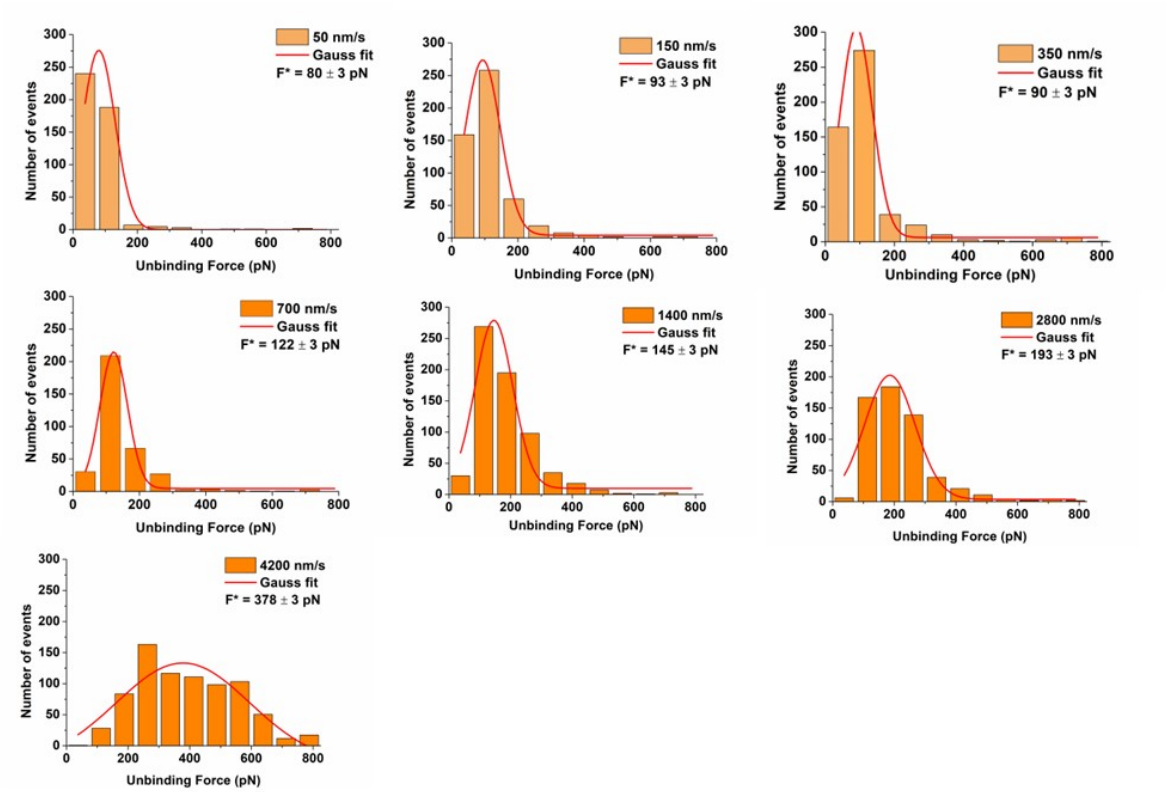

Figure S4. Histograms of the unbinding forces for the IsdB:(ββ)XL-Hb complex from AFS measurements carried out at increasing retraction velocities, using a binning of 75 nN. Each histogram was fitted with a Gaussian function (red curve) to determine the most probable unbinding force value (F*) from the peak maximum.

All the histograms, at both the binnings for both the IsdB:metHb and IsdB:(ββ)XL-Hb systems, are characterized by a single mode which can be well described by a single Gaussian curve. We note that, at the highest loading rates, the wider spread of the unbinding forces results into a lower statistics when a lower binning is used.

Fig.S5 shows the histograms of the IsdB:HbCO complex, at a only one binning since a rather low dispersion of unbinding forces is registered.

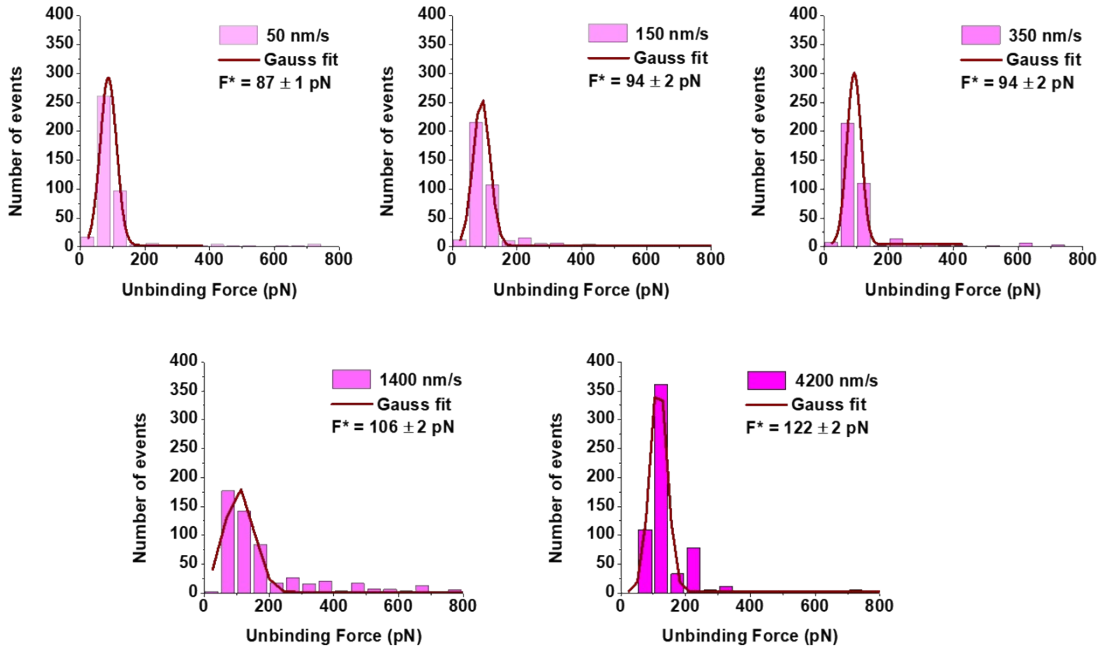

Figure S5 Histograms of the unbinding forces for the IsdB:HbCO complex from AFS measurements carried out at increasing retraction velocities, using a binning of 35 nN. Each histogram was fitted with a Gaussian function (red curve) to determine the most probable unbinding force value (F*) from the peak maximum.

Blocking experiments

To assess the specificity of the unbinding events detected in all the IsdB:Hb systems (IsdB:metHb, IsdB:(ββ)XL-Hb, and IsdB:HbCO) by AFS experiments (described in the main text), we have carried out blocking experiments by following the same procedure reported in refs. [1]. Briefly, we have collected force curves with an IsdB-functionalized tip, previously incubated with a solution containing the partner (Hb at 10 μM), against the Hb-substrate. The number of events at different unbinding forces, before and after blocking, is shown in Figs. S4-S6, for the three analyzed IsdB:Hb systems; blocking experiments having been carried out at a retraction velocity of 350 nm/s. The unbinding frequency values, calculated as the ratio of the number of events corresponding to specific unbinding processes over the total recorded events, before and after blocking, are also shown. In all the cases, we note that the histograms before and after blocking are characterized by almost the same shape, but with a reduced number of events in the latter case, in agreement with literature [2-4]. The reduction upon blocking ranges from 41% to 66%, witnessing the specificity of the binding events.

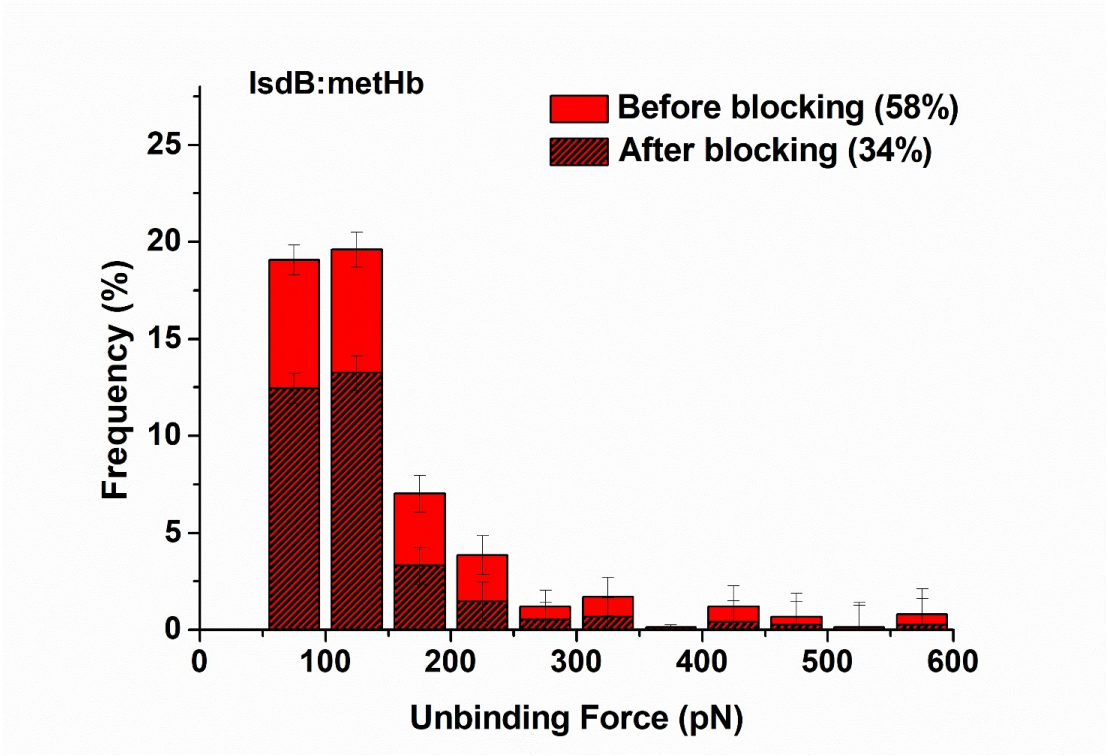

Figure S6. Histograms of the unbinding forces for the IsdB:metHb complex before (solid columns) and after (dashed columns) blocking, from AFS measurements carried out at a retraction velocity of 350 nm/s. The ratios (in percentage) of the number of events corresponding to specific unbinding processes over the total recorded events are reported.

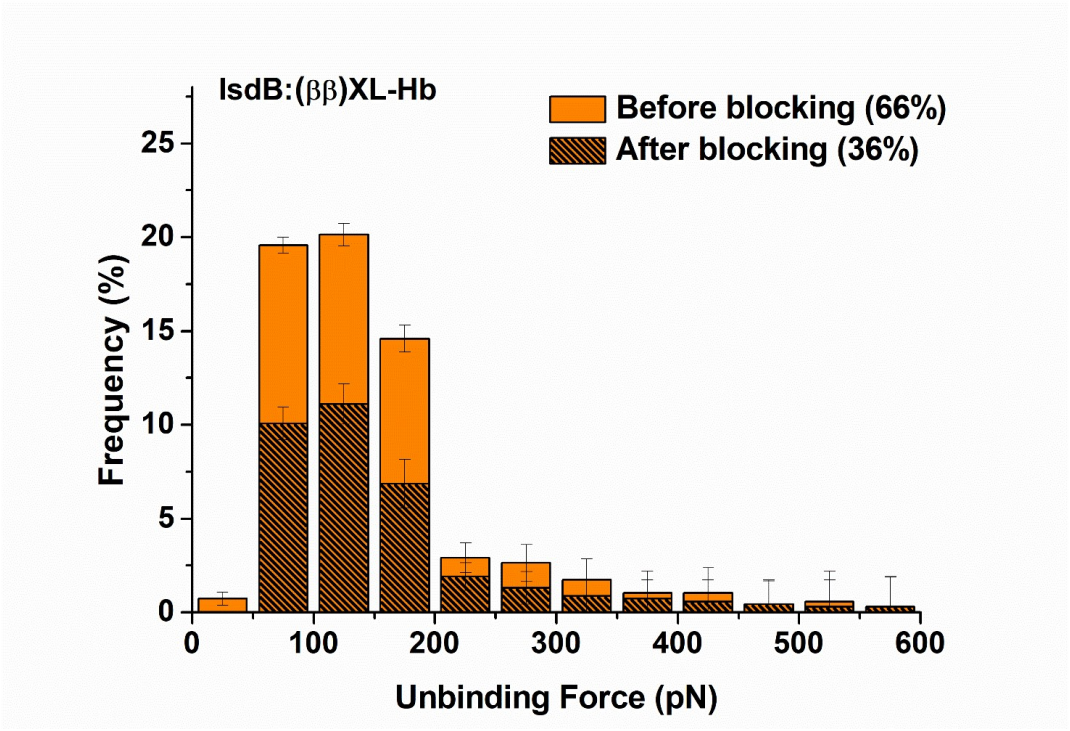

Figure S7. Histograms of the unbinding forces for the IsdB:(ββ)XL-Hb complex before (solid columns) and after (dashed columns) blocking, from AFS measurements carried out at a retraction velocity of 350 nm/s. The ratios (in percentage) of the number of events corresponding to specific unbinding processes over the total recorded events are reported.

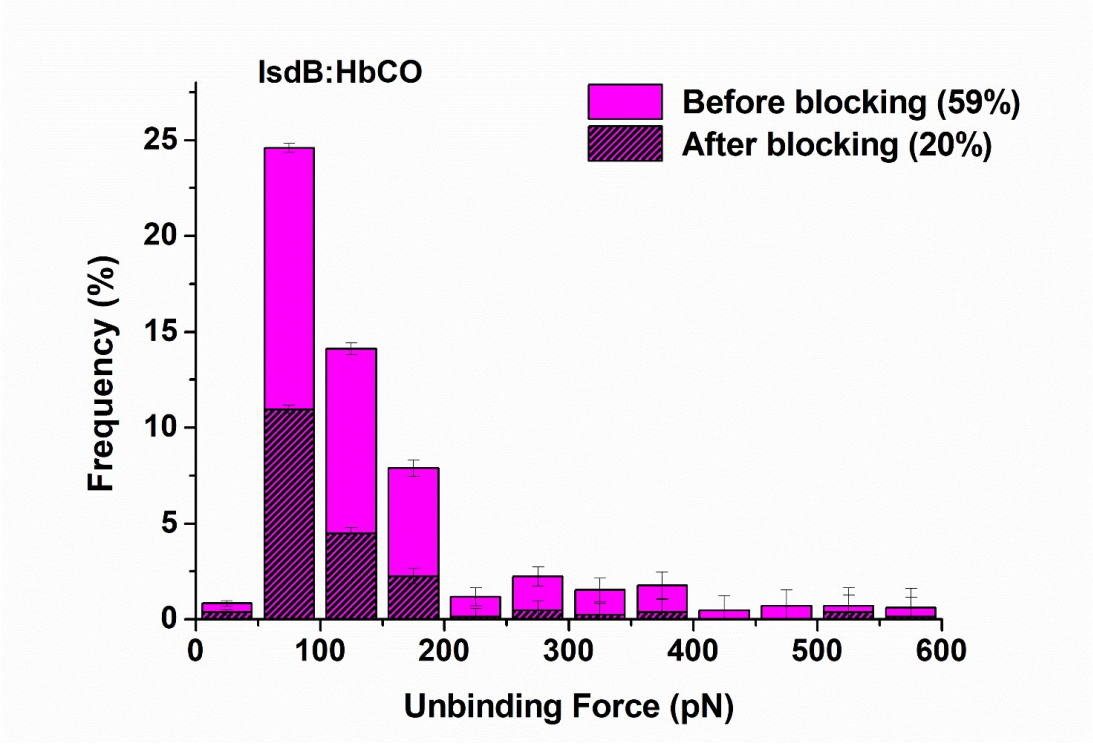

Figure S8. Histograms of the unbinding forces for the IsdB:HbCO complex before (solid columns) and after (dashed columns) blocking, from AFS measurements carried out at a retraction velocity of 350 nm/s. The ratios (in percentage) of the number of events corresponding to specific unbinding processes over the total recorded events are reported.

To further support the specificity, we have also analysed the rupture length, obtained by subtracting tip deflection from the distance between contact and unbinding, as described in refs.[2,5]. Fig.S9 shows the histogram of the rupture length before and after blocking, for the IsdB:metHb complex.

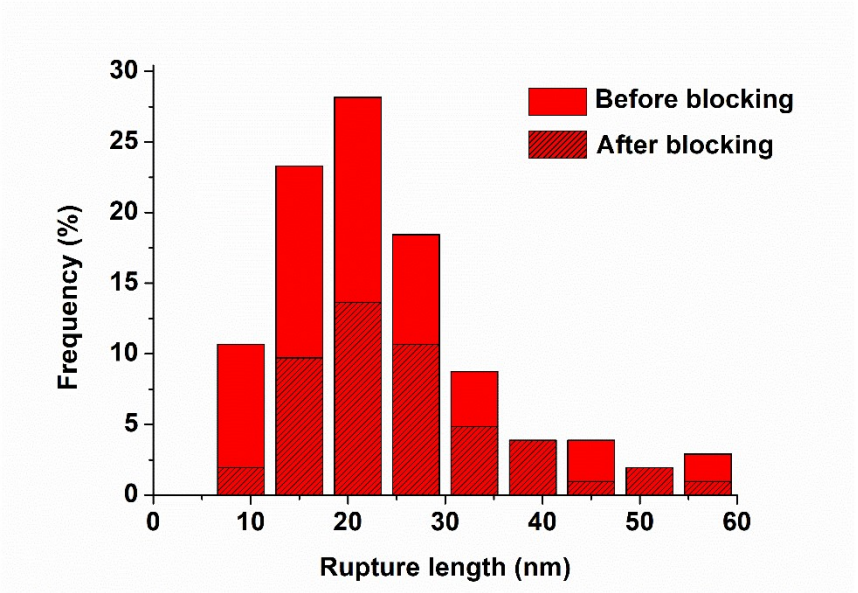

Figure S9. Histograms of the rupture lengths for the IsdB:metHb complex before (solid columns) and after (dashed columns) blocking, from AFS measurements carried out at a retraction velocity of 350 nm/s (from the same force curves used in Fig.S6.

Again, we note that the histograms before and after blocking are characterized by a single mode distribution almost the same shape, but with a lower number of events in agreement with what observed for the unbinding forces. Furthermore, the distribution is centred at about 25 nm, consistently with the used PEG linker and in agreement with what observed in the literature [2].

Analysis of the unbinding forces

Fig.S10 shows the most probable unbinding force as a function of the loading rate for the complex between IsdB and metHb; with the forces being derived from the unbinding forces histograms by using two different binnings. In both cases, we note a linear trend for loading rate values below about 30 nN/s, while a significant deviation from the initial linear trend occurs at higher loading rate values, irrespectively of the used binning.

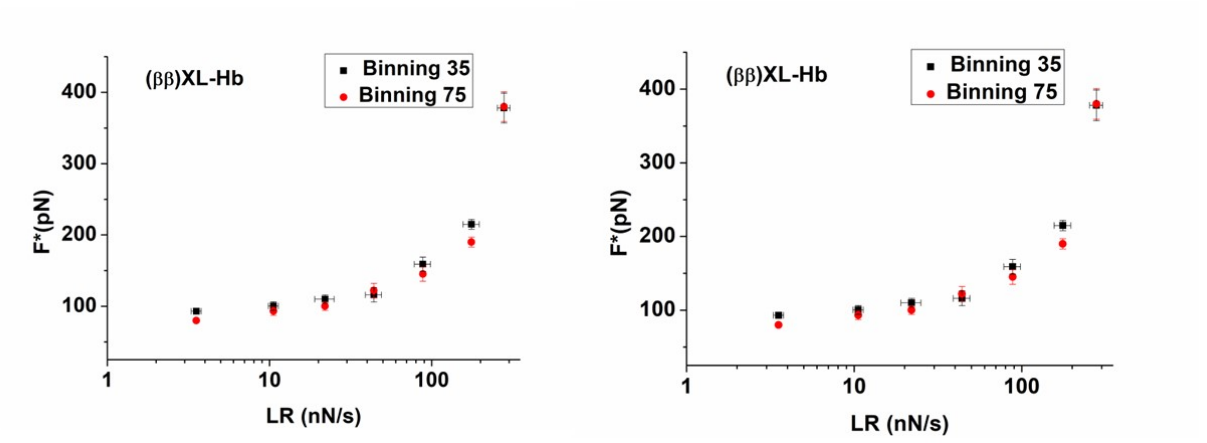

Figure S10. The most probable unbinding force vs. the logarithm of the loading rate for: A) the IsdB:metHb complex and B) the IsdB:(ββ)XL-Hb complex.

Generally, the linear trend can be put into relationship to the overcoming of a single barrier (without rebinding) and it can be described by the Bell-Evans model (BE) [6], in which the most probable

force, F*, as a function of the natural logarithm of the loading rate, r, can be expressed by the following expression:

$$F^* = \frac{k_B T}{x_\beta} \ln \frac{r\, x_\beta}{k_{off} k_B T} \tag{S1}$$

where k_B is the Boltzmann constant, T is the absolute temperature, k_{off} is the dissociation rate constant, and x_β is the width of the energy barrier along the direction of the applied force.

Our data cannot be globally fitted by the BE model, as evident from the red dash-dot line in Fig. S11. Successively, we have tested the hypothesis that two subsequent energy barriers should be overcome for a complete unbinding. Accordingly, two different linear trends should be present, each one described by the BE model but with different parameters. The resulting fitting curves, derived from data extracted from the lower binning, are shown in Fig.S11. As expected, below 30 N/s, data are consistent with a linear trend, and they can be well described by the BE model (continuous red line); the corresponding parameters being shown in Fig. S11 (red values):

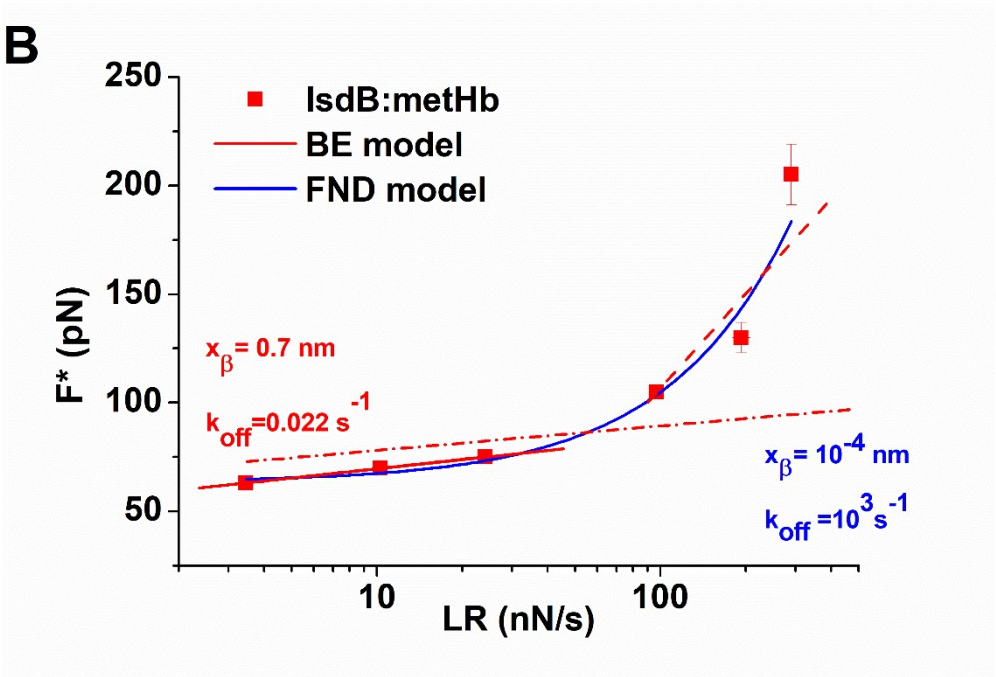

Figure S11. The most probable unbinding force vs. the logarithm of the loading rate for the IsdB:metHb complex. Red lines are the best fits of all or a part of data by the Bell–Evans model (Eq. S1): continuous line fitting of data for loading rate less than 30 nN/s; dashed line fitting of data for loading rate higher than 30 nN/s; dashed-dot line fitting of data for all loading rate values. Blue continuous line is the best fit by the Friddle-Noy-De Yoreo model.

The extracted parameters corresponding to continuous lines are reported. At higher loading rate values, instead, a fit by the BE model poorly describes the experimental trend (red dashed line). Such a result allows us to rule out the existence of two barriers to be overcome for a complete unbinding. In addition, we have taken into consideration the possible occurrence of rebinding and we have applied the Friddle-Noy-De Yoreo (FND) model, which assumes a first reversible binding followed by an irreversible one [7]. In this framework, the average unbinding force can be described by the following approximated expression [8]:

$$\langle F \rangle = f_{eq} + \frac{k_B T}{x_\beta} \ln \left[1 + \frac{r\, e^{-\gamma}}{k_{off}(f_{eq}) \frac{k_B T}{x_\beta}} \right] \quad \text{(S2)}$$

where f_{eq} is the force at which the dissociation rate and the association rate cross (related to the height of the energy barrier), γ is the Euler constant (0.577); the other parameters being the same as in Eq. S1. Generally, such a model predicts a non-linear increasing trend as far as higher loading rates are applied.

The fit of our data by Eq. S2 (continuous blue line) reproduces the increasing trend. However, the values of extracted parameters do not have a physical meaning. Indeed, $k_{off}=10^3$ s^{-1} is higher than the maximum observed value (about 600 s^{-1}), and, more importantly, $x_\beta=10^{-4}$ nm is an unrealistic value (see ref. [9]). Accordingly, the FND model cannot reliably reproduce our data and the corresponding description of data in terms of rebinding should be discarded.

We have also analysed the trend of the average unbinding forces as a function of the loading rate. From Fig.S12, we note that even in this case, the force trend exhibits a change by passing from low to high loading rates for IsdB:metHb and IsdB:(ββ)-XLHb and not the IsdB-HbCO, in agreement with the results shown in the Bell-Evans plot.

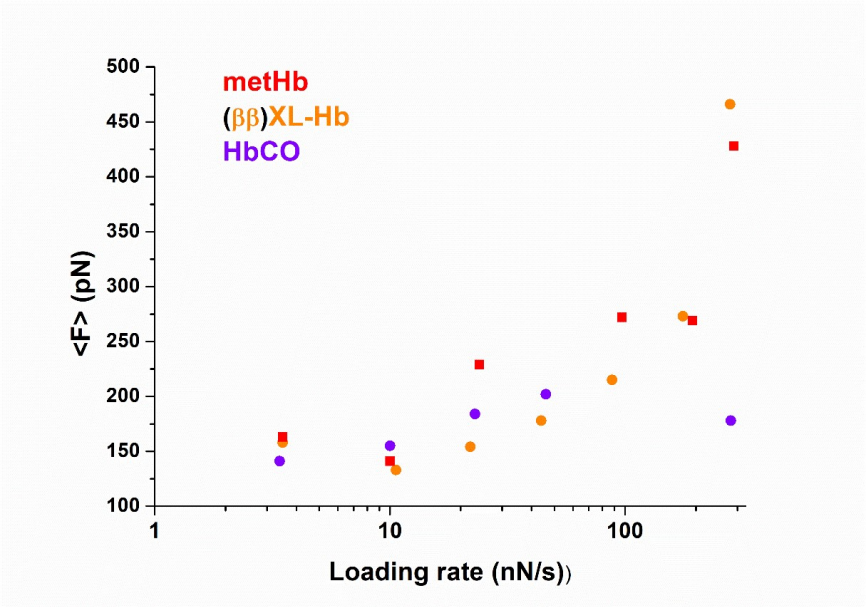

Figure S12. The average unbinding force vs. the logarithm of the loading rate for the three IsdB-Hb systems.

References

1. V. Botti, S. Cannistraro, A.R. Bizzarri. Interaction of miR-155 with Human Serum Albumin: An Atomic Force Spectroscopy, Fluorescence, FRET, and Computational Modelling Evidence. *International Journal of Molecular Sciences*. 2022, 23, 10728. https://doi.org/10.3390/ijms231810728
2. P. Hinterdorfer, W. Baumgartner, H.J. Gruber, K. Schilcher, H. Schindler. Detection and localization of individual antibody-antigen recognition events by atomic force microscopy. *Proc Natl Acad Sci U S A*. 1996, 93, 3477.
3. R. De Paris, T. Strunz, K. Oroszlan, H. J. Guentherodt and M. Hegner, Force Spectroscopy and Dynamics of the Biotin Avidin Bond Studied by Scanning Force Microscopy. Single Mol. 2000, 1, 285.
4. N. Berquand, D.G. Xia, B. H. Castner, N. L.Clare, V. Abbott,Y., Dupres, Y. Adriaensen, and Y.F Dufrêne. 2005. Antigen binding forces of single antilysozymeFv fragments explored by atomic force microscopy. *Langmuir*. 2005, 21, 5517.
5. W. Baumgartner, P. Hinterdorfer, W Ness, A. Raab, D. Vestweber, H. Schindler, D. Drenckhahn. Cadherin interaction probed by atomic force microscopy. *Proc. Natl. Acad. Sci.* USA, 2000, 97, 4005-4010.
6. E. Evans, Probing the relation between force-lifetime and chemistry in single molecular bonds. *Annu. Rev. Biophys. Biomol. Struct* **2001**, *30*, 105
7. R. W. Friddle, A. Noy and J. J. De Yoreo, *Proc. Natl. Acad. Sci. USA.,* 2012, 109, 13573–13578.
8. F. T. Hane, S. J. Attwood, Z. and Leonenko. Comparison of three competing dynamic force spectroscopy models to study binding forces of amyloid-β. *Soft Matter*, 2014, 10, 1924-1930.
9. A.R. Bizzarri and S. Cannistraro, (Eds). Dynamic Force Spectroscopy and Biomolecular Recognition. (Eds.). (2012). Dynamic Force Spectroscopy and Biomolecular Recognition (1st ed.). CRC Press.